DESIGN, SYNTHESIS AND EVALUATION OF ANTITUBERCULAR, ANALGESIC AND ANTI-INFLAMMATORY ACTIVITY OF NOVEL 1H-INDAZOLE DERIVATIVES

Rajesh B. Nanaware[1], Anuruddha R. Chabukswar[2]*, Prajakta V. Adsule[3]

Article History: Received: 27.05.2023 Revised: 09.06.2023 Accepted: 27.06.2023

Abstract

Despite decades of focused effort to eradicate it, TB still remains and is becoming more resistant to treatment. Due to the long duration of treatment for these diseases, their continual geographic spread, their rising level of drug resistance, as well as the toxicity and side effects connected with the currently available drugs, the development of novel antitubercular medications and regimens is necessary. In this study we are targeting the Indazole nucleus which offers wide substitution pattern on the ring and explored for the development of the newer efficient and safe molecules against tuberculosis, analgesia and inflammation. Here, some N-substituted indazoles were synthesized by using HATU as a coupling agent, which inhibits Enoyl acyl carrier protein reductase which is essential for the synthesis of mycolic acid in the tubercle bacilli. The molecular docking studies were found to be potentially binds to 2AQK enzyme. The results of the MD simulation showed that the test compound BOT was significantly stable in the Enoyl-ACP reductase-2AQK active site. The compound BOT-2AQK post-dynamic MM-GBSA analysis revealed substantial binding affinities with each of its chosen targets. Biological evaluation of synthesized compounds showed that, mycobacterium tuberculosis is effectively inhibited by the compound BDF, BOT, and BPM, while the compound BPT with the p-toluene group has the strongest analgesic and anti-inflammatory activity.

***Keywords*:** Enoyl-acyl carrier protein reductase, 1H-Indazole, Mycobacterium tuberculosis, Molecular docking and MD simulations, Analgesic and anti-inflammatory.

[1,2,3]School of Health Sciences and Technology, Department of Pharmaceutical Sciences, Dr. Vishwanath Karad MIT-World Peace University, Pune-411038, Maharashtra, India.

*Corresponding author: E-mail: **anuruddha.chabukswar@mitwpu.edu.in**

DOI:10.48047/ecb/2023.12.si8.486

1. Introduction

The COVID-19 pandemic still negatively affects both the burden of TB disease and provision to TB diagnosis and treatment. Global TB objectives are not being met at pace, and progress made in the years leading up to 2019 has slowed, stopped, or even reversed. The largest global decline in the reported number of people having a new TB diagnosis was the most noticeable and immediate effect. This dropped to 5.8 million in 2020 (-18%) from a peak of 7.1 million in 2019, returning to the level last seen in 2012. A modest rebound occurred in 2021, reaching 6.4 million (the level of 2016–2017). In 2021, an estimated 10.6 million individuals (95%UI: 9.9-11 million) developed TB, an increase of 4.5% over the previous year's 10.1 million (95%UI: 9.5–10.7 million) in 2020. The number of new cases of tuberculosis (TB) per 100,000 people increased by 3.6% between 2020 and 2021, reversing annual decreases of roughly 2% for the most of the preceding two decades. The number of new cases of rifampicin-resistant TB (RR-TB) or MDR TB (multidrug resistant TB) is predicted to reach 450 000 (95% UI: 399 000-501 000) in 2021, adding to the burden of drug-resistant tuberculosis (DR-TB) [1]. TB still exists and is getting more resistant to treatment despite decades of concerted effort to eradicate it. The discovery of innovative antitubercular medications and regimens is required due to the prolonged period of treatment for these illnesses, their continuous geographic spread, and their increasing level of drug resistance as well as toxicity and adverse effects associated with the presently available drugs [2].

Presently we are targeting the Indazole nucleus which offers wide substitution pattern on the ring and can be further explored for the development of the newer

efficient and safe molecules. Indazoles are found to have a wide range of biological activities such as analgesic and anti-inflammatory [3-4], antimicrobial [5], anticancer [6-7], antiviral [8], antitubercular [9-11], antiplatelet [12] and 5-HT6 antagonists [13].

In this context, our study focuses on the approach of rational drug design in the search of newer molecules against tuberculosis. Enoyl-acyl carrier protein reductase (InhA) enzyme involved in the mycolic acid synthesis has been targeted for the development of some useful molecules. The compounds with relatively higher docking scores were selected, and the stability of their interactions with the targetprotein was determined by MD simulation study and to calculate the binding free energies of selected complexes, the MM-GBSA method was employed. Antitubercular activity and anti-inflammatory dual action were evaluated by using MABA assay and carragenan induced rat paw edema method respectively.

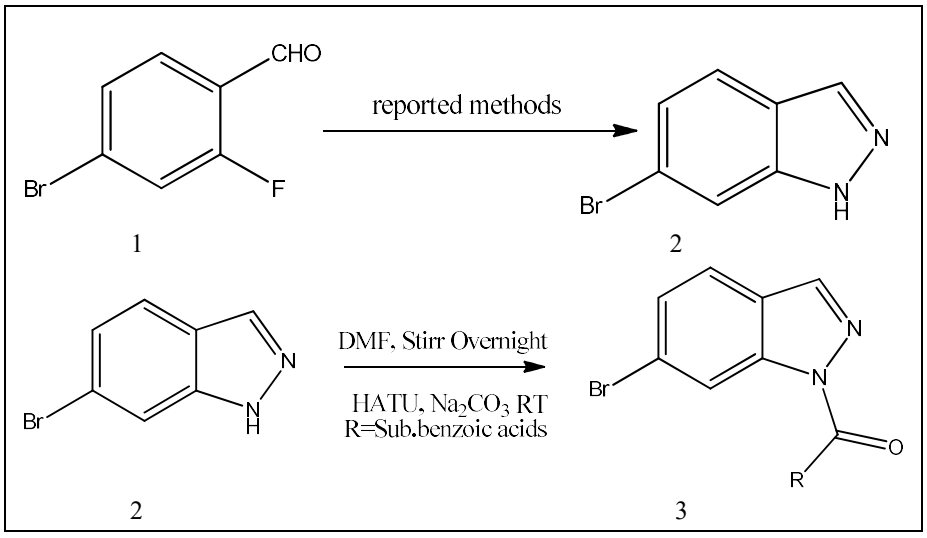

Figure 1. Synthesis scheme

2. Materials and Methods

2.1 Chemistry:

All the solvents used in the reaction and for purification were distilled out prior to use. By using thin-layer chromatography (TLC) using silica gel 60 GF254 Merck pre-coated aluminum sheets and eluting the samples with ethyl acetate: hexane 3:7 (vol. parts), the novel compounds purity was examined. Melting points were determined using a Veego melting point device and were uncorrected. A Jasco FT/IR-4600 spectrometer was used to measure IR spectra. Using CDCl3 as the solvent, ^{1}H NMR and ^{13}C NMR spectra were recorded at 500 MHz on a Bruker spectrometer.

2.2 Molecular Docking:

2.2.1 Construction of Ligand:

12 newly developed compounds with an indazole scaffold were made using the ACD/ChemSketch software. The Open Babel GUI was used to convert all of the 3D structures into PDB file format [14]. UCSF-Chimera software was used to minimize all of the structures energy [15] and then converted into PDBQT using Autodock tools 4.2.6. [16-17].

2.2.2 Preparation of Receptor:

The protein data bank (PDB) (https://www.rcsb.org/) was used to retrieve the Enoyl-ACP reductase enzymes 3D crystal structure, PDB ID: 2AQK [18-19]. Polar hydrogen and Kollman charges were added to the proteins after water molecules, ions, and other ligands had been taken out. After allocating AD4 charges, PDBQT files for the receptor protein were created using the AutoDock Tools (ADT) graphical user interface tool.

2.2.3 Grid generation and molecular docking:

In order to generate the grid parameter (.gpf) files, grid box size was adjusted to 102×104×112 (0.5Å spacing) for 2AQK protein. The genetic search Lamarkain algorithm was used in the docking investigation to conduct 10 docking runs for each ligand in an effort to determine the

ligands ideal conformational space. The number of evaluations and the generations were set to 27000 and 2500000, respectively. For analyzing close intramolecular interactions with the receptor, the ligand conformation that had the greatest amount of binding energy was selected.

2.2.3 Molecular dynamics simulation (MD) study:

Using the Desmond 2020.1 from Schrodinger, LLC, MD simulation investigations were performed on the docked complexes 2AQK+BOT, 2AQK+NAI, and 2AQK-apo [20]. In this system, the OPLS-2005 force field [21–23] and explicit solvent model with SPC water molecules [24] were applied. For stimulation of physiological environment, 0.15M of sodium chloride solution was added to the system along with Na+ ions to balance the charge. To retrain over the protein complex, using NVT ensemble for 100ps the system was initially equilibrated. This was followed by a 12-ps NPT ensemble short run equilibration and minimization. The Nose-Hoover chain coupling scheme [25] was used to set up the NPT ensemble, which was maintained throughout all simulations at a temperature of 27^{o}C, a relaxation time of 1.0ps, and a pressure of 1bar. The Martyna-Tuckerman-Klein chain coupling method Pressure was controlled using the [26] barostat method with a 2 ps relaxation time. The radius for the coulomb interactions was set at 9Å, and the long-range electrostatic interactions were calculated using the particle mesh Ewald method [27]. Bonded forces were estimated for each trajectory using the RESPA integrator for a time step of 2fs. To monitor the MD simulations stability, the root mean square deviation (RMSD), radius of gyration (Rg), root mean square fluctuation (RMSF), and solvent accessible surface area (SAS Area) were computed.

2.2.4 Analysis of binding free energy: Molecular mechanics and generalized born

surface area (MM-GBSA) calculations were used to determine the binding free energies of each complex. The MM-GBSA binding free energy was estimated by the python script thermal_mmgbsa.py in the simulation trajectory and the final 50 frames of the OPLS 2005 force field with a 100-step sample size. Using the additivity concept, which involves adding up every individual energy module such as a covalent, hydrogen bond, van der Waals, self-contact, lipophilic, solvation, and stacking of ligand and protein, the binding free energy of Prime MM-GBSA (kcal/mol) was calculated. ΔG_{bind} is calculated by following equation:

$$\Delta G_{bind} = \Delta G_{MM} + \Delta G_{Solv} - \Delta G_{SA}$$

2.2.5 Investigation of Drug-likeness and ADMET properties:

In the current work, the Lipinski's parameters and ADMET properties of proposed compounds were predicted using a free online database server called SwissADME [28–30]. An efficient drug's transport through the blood-brain barrier was estimated using topological polar surface area (tPSA) [31–32].

2.2.6 Antimycobacterial activity:

Using MABA assay, the anti-mycobacterial activity of compounds was examined against M. tuberculosis. In order to reduce the amount of medium that evaporates out during incubation, 200µl of sterile deionized water was added to all of the sterile 96-well plates outside perimeter wells. Compounds were serially diluted on the 96-well plate after addition of 100µl of Middlebrook 7H9 broth. The final drug concentrations measured were between 100 and 0.2 g/ml. The plates were covered and sealed with parafilm, then incubated for five days at 37 °C. Following this, the plate received 25µl of a freshly produced 1:1 mixture of 10% tween 80 and Almar Blue reagent, which was then applied. The well's pink colour was interpreted as growth whereas the blue colour was interpreted as no bacterial growth. MIC was referred as the lowest drug

concentration that prevented the colour changing from blue to pink.

Standard Strain: Mycobacterium tuberculosis ATCC No. 27294 (Vaccine strain: H37Rv): MIC of reference compound isoniazid, ethambutol, pyrizinamide, rifampicin and streptomycin were found to be 1.6, 1.6, 3.1, 0.8 and 0.8 µg/ml respectively.

2.2.7 Anti-inflammatory activity:

Experimental design:

After getting ethical clearance from IAEC; animals will be obtained from Crystal Life Sciences Pune, 7-days before the commencement of the study.

Animals will be maintained in registered animal houses in polypropylene cages at a controlled room temperature of 22 ±1°C and a relative humidity of 60–70% (198/PO/Re/S/2000/CPCSEA).They will be maintained with standard pellet diet Nutrivet Life Sciences and water (ad libitum). Animals will be divided into 8 different groups of 06 animals in every group. Test compound will be administered orally to the respective group of animals at different dose levels. Rats were given an overnight fast with free access to water prior to the studies. Animals behaved normally during the experiment.

2.2.8 Carrageenan-induced Rat Paw Edema:

Wistar rats (150-200 gm) will be used for this study. 0.1 ml 1 % w/v of carrageenan in normal saline (0.9% w/v NaCl solution) will be injected into the subplanter region of the left hind paw of rat. Right hind paw of each rat will be taken for control. Animals will be divided into 8 groups containing 6 in each. Vehicle/Test/standard compounds will be administered after 1 h of the injection of carrageenan. A plethysmometer was used to measure the paw volume at 0 h (Vc) (before Carrageenan injection) and 30min.,1, 2, 3, 4, 6,12 and 24h later (Vt) (after Carrageenan injection). Each rats paw swelling was measured, and the edema value was determined as the difference between Vt

and Vc. The following formula was used to determine the % inhibition of edema:

$$Vc-Vt/Vc \times 100$$

2.2.9 Analgesic Activity:

Swiss mice that weighed between 25 and 35 g were chosen for the analgesic activity and were kept in a uniform laboratory environment, fed a commercial diet, and provided with water ad libitum, during the experiment. Animals were purchased from Crystal Life Sciences Pune.

Hot plate reaction time in mice:

Animals will be divided into 8 groups containing 6 in each. Animals will be placed on a hot plate that is kept at a constant temperature (55 ± 0.5 °C), and basal reaction time will be measured by watching for the animal's first hind paw lick or jump response (whichever occurs first). Animals typically show this response within 6–8 seconds. To protect the paws, a 15 second cut-off time is observed. To validate that the mice behave normally, three basal reaction times for each mouse will be recorded with a 5-minute interval. Pentazocine/test chemical will be delivered, and at 15, 30, 60, 90, 120, 150, 180, and 210 minutes after the treatment, the animal response times on the hot plate will be noted. At each time interval, the percentage increase in reaction time (as an indicator of analgesia) will be calculated.

3. Results and Discussion

3.1 Synthesis of 1H-indazole:

6-bromoindazole was prepared following literature methods [33-34].

Procedure for the synthesis of ^{1}H-indazole derivatives:

To a stirred solution of 6-bromo-1H-indazole (1equivalent) and DMF, 1equivalent 3,4-difluorobenzoic acid, BDF, 4-methylbenzoic acid, BPT, 4-nitrobenzoic acid, BPN, 2-methylbenzoic acid, BOT, 2-ethoxyacetic acid, BETX,4-(trifluoromethyl) benzoic acid, BCF, 1.1quivalents HATU and 2 equivalents Na_2CO_3 was added. The reaction mixture was stirred at R.T. for overnight. The solid product formed was collected by filtration. Indazole derivatives

were produced after the residue was purified by filtering it through a pad of silica, and these compounds were then validated by FT-IR, ^{1}H NMR, ^{13}C NMR, and Mass spectroscopy.

1. ***Synthesis of (6-bromo-1H-indazol-1-yl) (3,4-difluorophenyl) methanone, BDF:***

Yield: 72%; m.p.160 °C. IR (KBr, cm^{-1}): ν 3115, 3059, 2920, 2856, 1686, 1611, 1575, 1514, 1423, 1339, 1195, 1114, 1082, 1054, 962, 908, 854, 814, 777, 738, 655, 558, 445, 430.^{1}H NMR (500MHz, $CDCl_3$, δ (ppm)): $C_{14}H_7BrF_2N_2O$, 8.18(s,1H), 8.77(s,1H), 7.66(d,1H), 7.54(s,1H), 7.55(s, 1H), 7.34(m, 1H), 7.32(m,1H). ^{13}C NMR (500MHz, $CDCl_3$, δ (ppm)): 165.7, 154.3, 152.2, 148.7, 140.3, 129.3, 128.7, 124.8, 124.5, 122.0, 121.1, 121.0, 119.1, 117.0. LCMS: *m/z* 377.7 [M + K].

2. Synthesis of (6-bromo-1H-indazol-1-yl) (p-tolyl) methanone, BPT:

Yield: 70%; m.p.105°C. IR (KBr, cm^{-1}): ν 3229, 3200, 3173, 3083, 3030, 2919, 2858, 1736, 1686, 1605, 1403, 1361, 1292, 1261, 1116, 1073, 1040, 959, 912, 883, 821, 785, 739, 694, 589, 478. ^{1}H NMR (500MHz, CDCl3, δ (ppm)): $C_{15}H_{11}BrN_2O$, 8.79 (s,1H), 8.15 (s,1H), 7.99 (q,1H), 7.64(t,2H), 7.53(m,1H), 7.33(t,2H), 2.45 (s,3H). ^{13}C NMR (500MHz, $CDCl_3$, δ (ppm)): 168.1, 143.3, 140.9, 139.6, 131.1, 129.8, 128.7, 128.3, 124.8, 124.1, 121.8, and 119.0. LCMS: *m/z* 314 [M $^{+}$].

3. ***Synthesis of (6-bromo-1H-indazol-1-yl) (4-nitrophenyl) methanone, BPN:***

Yield: 75%; m.p. 212°C. IR (KBr, cm^{1}): ν 3363, 3109, 3049, 2940, 1693, 1602, 1523, 1485, 1414, 1352, 1294, 1221, 1159, 1116, 1079, 989, 913, 855, 805, 785, 717, 619, 502, 427. ^{1}H NMR (500MHz, $CDCl_3$, δ (ppm)): $C_{14}H_8BrN_3O_3$, 8.80 (d, 2H), 8.38 (s, 1H), 8.23 (d, 2H), 8.01 (s, 1H), 7.68(t, 1H), 7.58 (m, 1H). ^{13}C NMR (500MHz, $CDCl_3$, δ (ppm)): 166.1, 149.8, 140.9, 140.6, 138.4, 131.9, 129.1, 125.0, 124.7, 123.1, 122.1, and 119.0. HRMS: *m/z* 367.9 [M + Na].

4. ***Synthesis of (6-bromo-1H-indazol-1-yl) (o-tolyl) methanone, BOT:***

Yield: 74%; m.p.155 °C. IR (KBr, cm^{-1}): ν 3426, 3371, 3180, 3104, 3059, 3026, 2960, 2924, 2857, 2732, 2647, 2505, 2447,1693, 1605, 1579, 1482, 1401, 1362, 1344, 1189, 1158, 1118, 1076,1042, 868, 779, 655, 619, 596, 548, 425.^{1}H NMR (500MHz, $CDCl_3$, δ (ppm)): $C_{15}H_{11}BrN_2O$, 8.83(s,1H),8.10 (d,1H),7.64(m,1H),7.60(t,1H),7.58(m,1H),7. 49(m,1H),7.46(t,1H),7.31(d, 1H), 2.35 (s,3H). ^{13}C NMR (500MHz, $CDCl_3$, δ (ppm)): 169.8, 144.3, 144.2, 136.5, 130.83, 130.6, 128.57, 128.53, 125.3, 124.3, 121.9, 118.8, and 19.7. LCMS *m/z:* 315 [M + H].

5. Synthesis of 1-(6-bromo-1H-indazol-1-yl)-2-ethoxyethanone, BETX:

Yield: 79%; m.p.120 °C. IR (KBr, cm^{-1}): ν 3433, 3380, 3330, 3313, 3294, 3246, 3215, 3172, 3111, 3073, 2975, 2935, 2902, 2794, 2674, 1727, 1605, 1541, 1486, 1473, 1411, 1329, 1281, 1144, 1110, 1039, 1005, 936, 852, 808, 773, 750, 688, 626, 593, 426. ^{1}HNMR (500MHz, $CDCl_3$, δ (ppm)): $C_{11}H_{11}BrN_2O$, 8.83(s, 1H), 8.67 (s, 1H), 7.64 (q,1H), 7.62 (t,2H), 7.54 (m,1H), 7.44 (t,2H), 2.35 (s,3H). ^{13}C NMR (500MHz, $CDCl_3$, δ (ppm)): 169.8, 139.9, 139.7, 128.4, 124.6, 124.4, 121.9, 118.3, 69.2, 67.5 and 15.1. LCMS: *m/z* 307.5 $[M + Na]^+$

6. *Synthesis of (6-bromo-1H-indazol-1-yl) (4-(trifluoromethyl) phenyl) methanone, BCF:* Yield: 79%; m.p.120 °C. IR (KBr, cm^{-1}): ν 3380, 3330, 3294, 3246, 3215, 3172, 3111, 3073, 2975, 2935, 2902, 2794, 2674, 1727, 1605, 1541, 1486, 1411, 1329, 1281, 1144, 1110, 1039, 936, 852, 773, 626, 593, 426. ^{1}H NMR (500MHz, $CDCl_3$, δ (ppm)): $C_{15}H_8BrF_3N_2O$, 8.81(t,1H), 8.16 (d,1H), 7.80 (d,2H),7.67 (d,2H),7.65 (d,1H),7.58 (m,1H). ^{13}C NMR (500MHz, $CDCl_3$, δ (ppm)): 165.0, 144.1, 139.4, 136.8, 133.8, 130.2, 125.6, 125.1, 124.1, 124.0, 122.5, 120.9 and 113.9.

3.2 Molecular docking: Out of 12 compounds evaluated against 2AQK, the following compounds had the highest binding energies when compared to the isoniazid: **BOT** exhibited highest negative binding energy -8.49kcal/mol and showed H- bond interaction with Lys165 amino acid residue and their bond distance 5.56 Å. It formed C-H bond with Asp148 and Gly96 amino acids. It showed alkyl bond interactions with Pro193 and π-alkyl interaction with Tyr158, Phe149, and Ala191, Met147 and π-σ bond with Met161 and halogen bond with Met199 amino acids. Followed by **BPN** showed binding energy value of **-8.35** kcal/mol and 3-conventional H-bond interactions were observed with Ser20, Thr196 and Ile21 and 2.98, 4.46 and 4.98 Å bond distances respectively. Besides H-bonds, it showed π-π-staked bond with Phe41 amino acid residue. It also formed π-alkyl bond interactions with Ile122 and Phe41 amino acids. The binding interactions between these 2AQK and indazole derivatives were shown in Table 1 and Figure 2.

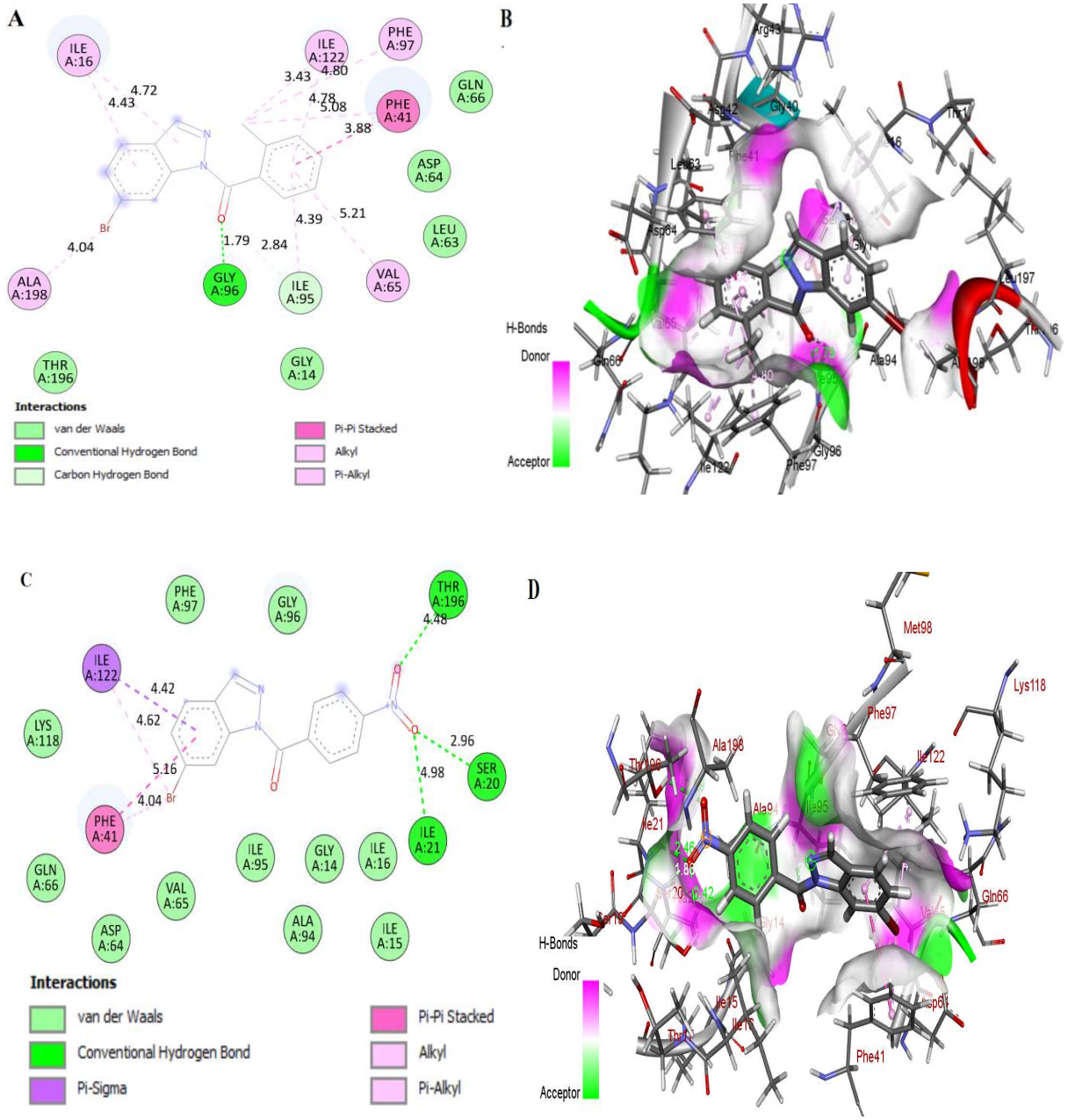

Fig.2 A & B) 2D & 3D Complex of BOT-2AQK C & D) 2D & 3D Complex of BPN-2AQK

Table 1. Interaction of the best binding compounds with 2AQK binding site residues:

Compd Code	Binding Energies (kcal/mol)	H-bonds	Angle of Bond (Å)	Hydrophobic and other interactions
BCF	-8.25	Gly96	4.17	Ala94, Phe41, Ile95, Ile122, Val65, Ala198, Ile21, Ser20, Thr196, Leu197, Ile16, Phe97, Asp64, Leu63, Gly14.
BPF	-7.83	Gly96, Val65	3.16, 4.83	Ile95, Phe41, Ile122, Asp64, Ile16, Ile95,Ala198,Thr196,Phe97,Gln66.
BOM	-7.77	Gly96	3.08	Phe41, Ile122, Ile16, Ala198, Phe97, Ile95, Thr196, Thr97, Asp42, Ilu63, Asp64, Val65, Gln66, Lys118.
BMT	-8.24	Gly96	2.76	Phe41, Ile122, Val65, Ile95, Ile16, Ala198, Thr196, Asp64, Leu63, Asp42, Gln66, Phe97.
BPT	**-8.31**	Gly96	3.22	Phe41, Ile122, Phe97, Ile16, Ile95, Asp64, Val65, Gln66, Ala94, Ser20, Thr196, Ala198.
BDF	-8.18	Gly96, Val65	3.87	Asp64, Ile95, Phe41, Ile122, Ilu63, Ile16, Ala198, Thr196, Phe97, Gln66.
BOT	**-8.49**	Gly96	1.79	Asp64,Ala198, Gly14, Val65, Thr196, Ile95, Leu63, Phe41, Gln66, Phe97, Ile122, Ile16
BPN	**-8.35**	Ser20, Thr196, Ile21	2.98, 4.46, 4.98	Phe41, Ile122, Ile95, Phe97, Gly96, Ile16, Ile15, Gly14, Ala94, Gln66, Asp64, Val65, Lys118.
BETX	-6.32	Gly14, Ile95	3.96, 4.29	Phe41, Ile122, Val65, Phe97, Gly96, Ala94, Thr196, Ile21, Ala22, Ser20, Ile15, Ile16, Asp64.
BBN	-8.26	Gly14, Ile95	3.80, 4.22	Gln66, Phe41, Ile122, Ala198, Ile16, Thr196, Ile21, Ser20, Ala94, Val65, Asp64, Lys118, Gly96.
BDP	-7.75	Thr196	4.39	Phe149, Ile16, Asp42, Phe41, Gly14, Ile95, Ala94, Gly96, Met147, Lys165, Asp148, Ala191, Ile194, Pro193, Gly192, Ala198
BPM	-7.66	Ile95	3.10	Ile122, Phe97, Phe41, Val65, Ile21, Gly96, Ala198, Thr196, Ser20, Ile16, Ala22, Gly14, Ile15, Ala94, Lys118, Gln66, Asp64.
INH	-5.21	Gly96, Val65	3.35, 3.71	Ile95, Ile122, Phe41, Phe97, Gln66, Asp64

3.3 Molecular Dynamics Simulation (MDS):

Simulations (MD) and experiments were employed in order to investigate the stability and convergence of 2AQK+BOT, 2AQK+NAI complexes and 2AQK-Apo protein. The root mean square deviation (RMSD) results demonstrated that the 100 ns simulation produced a stable conformation. The root mean square deviation (RMSD) of 2AQK+BOT Cα-backbone was found to be very high 3.5 Å but when it was coupled to NAI, RMSD was found to be 3.2 Å (Figure 3A). While the other apo protein 2AQK Cα-backbone the total RMSD has depicted to be 3.4 Å (Figure 3A). A good convergence and stable conformation was observed only for 2AQK+NAI complex. The 2AQK+BOT protein showed strong spikes of fluctuation in the RMSF plot (root mean square fluctuations); at residues 90-135, this might be a result of the residues increased flexibility. For the entire 100 ns simulation, the remaining residues fluctuated less (Figure 3B). While NAI exhibited similar pattern of fluctuation as of BOT (Figure 3B) but apo 2AQK exhibited large numbers of fluctuations, at 10-20, 47-54, 90-134, 155-57, 180-230 residues indicating that the amino acid conformations were flexible of those residues (Figure 3B). As a result, one can deduce, based on RMSF plots, that the structures of proteins having higher flexibility Apo-protein while BOT and NAI bound conforms more rigid structures during the simulation process.

The radius of gyration is a measurement that can be used to determine how compact the protein is (Rg). In this instance, the 2AQK+BOT Cα-backbone displayed a radius of gyration (Rg) that was consistently located between 18.2 and 18.3 Å. (Figure 3C). While NAI bound 2AQK exhibited lowering of peak from 18.3 to 18.3 Å and apo protein exhibited much lowering of peak upto from 18.2 to 18.1 Å (Figure 3C). The gyration (Rg) of a protein is at an all-time high level of stability when it is in its ligand-bound state. Lowering of peak indicate the highly compact structure. It suggests a complex that is highly interconnected and stable when there are a number of H-bonds between the ligand and the protein. During a simulation lasting one hundred nanoseconds, the number of H-bonds that exist between 2AQK and BOT, NAI and 2AQK are remained statistically significant (Figure 3D). It has been demonstrated that 2AQK and BOT have a number of hydrogen bonds with one another that is equal to the average, which is 2 (Figure 3D). Between NAI and

2AQK, the average numbers of H-bonds are observed to be 8 numbers (Figure 3D).

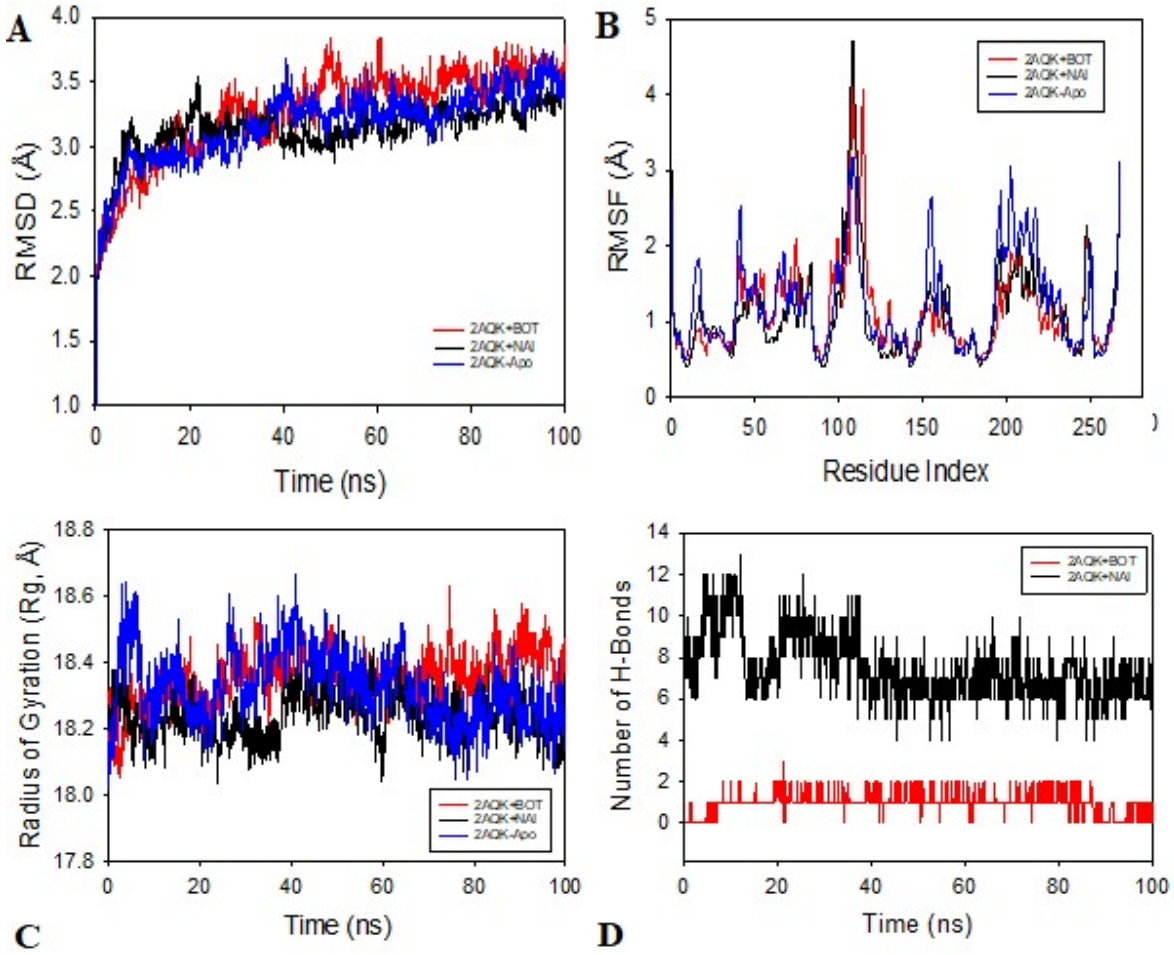

Figure 3. MD simulation analysis (100 ns trajectories) of (A) Cα backbone of 2AQK+BOT (red), 2AQK+NAI (Black) and 2AQK-Apo (Blue) (B) RMSF of Cα backbone of 2AQK+BOT (red), 2AQK+NAI (Black) and 2AQK-Apo (Blue). (C) Radius of gyration (Rg) of Cα backbone of 2AQK+BOT (red), 2AQK+NAI (Black) and 2AQK-Apo (Blue). (D) Formation of hydrogen bonds in 2AQK+BOT (red), 2AQK+NAI (Black) and 2AQK-Apo (Blue)

3.4 Calculation susing Molecular Mechanics Generalized Born Surface Area (MM-GBSA):

The MD simulation was used to determine the binding free energy and other energy in the form of MM-GBSA for 2AQK+BOT and 2AQK+NAI. According to the data, G_{bind}Coulomb, G_{bind}vdW, and G_{bind}Lipo appeared to have the biggest impact on the stability of the simulated complexes. On the other hand, G_{bind}Covalent and G_{bind}SolvGB were responsible for the opposite effect. In the complex of 2AQK+NAI, we found that the binding free energy was higher (more negative) than 2AQK+BOT. These findings substantiated that BOT has potential,

showed that it is effective in binding to the protein of choice, and revealed that it is capable of forming stable complexes of protein and ligand.

Table 2. Estimated by MM-GBSA: binding free energy components of the 2AQK+BOT and 2AQK+NAI:

Energies (kcal/mol)	2AQK+BOT	2AQK+NAI
ΔG_{bind}	-46.5±2.37	-99.52±4.22
ΔG_{bind}Lipo	-15.43±0.60	-14.93±0.73
ΔG_{bind}vdW	-36.25±1.34	-75.91±2.91
ΔG_{bind}Coulomb	-7.23±1.97	-46.82±4.81
$\Delta G_{bind}H_{bond}$	-0.40±0.12	-3.79±0.33
ΔG_{bind}SolvGB	13.47±1.09	35.82±4.10
ΔG_{bind}Covalent	0.51±0.44	8.17±2.34

4. Biological Evaluation

4.1 Antimycobactrial activity:

When the antimycobacterial activity of the synthesized indazole derivatives was tested in vitro using MABA at drug concentrations ranging from 0.8 g/ml to 100 g/ml against the reference strain Mycobacterium tuberculosis H37Rv (Table 3), it was discovered that the compounds were bactericidal in nature.Structure–activity relationship of compounds with respect to their antitubercular activity showed that compounds with 4-methyl benzoic acid, BOT, difluoro- benzoic acid, BDF and 4-methoxy benzoic acid, BPM substituted at 1 position of indazole scaffold were identified as the most potent molecules with MIC 6.25µg/ml.The other synthesized derivatives BCF, BPN and BETX displayed antimycobacterial activity with MIC 12.5µg/ml. Compounds BPT, BBN and BDP showed Antitubercular activity with MIC 25µg/ml and BPF, BOM and BMT were found to have MIC 50µg/ml.

From the above results it is demonstrated that the synthesized indazole derivatives are showing good antitubercular activity. Further the compounds showing promising have been tested for their antimicrobial activity and were found to be good antimicrobial agents.

Table 3: Synthesized compounds represented with substitutions along with their anti-tubercular activity:

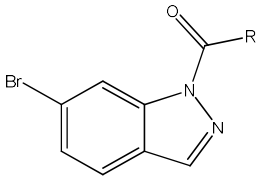

Compd.	R	H37Rv MIC (µg/ml)	Compd.	R	H37Rv MIC (µg/ml)
BCF	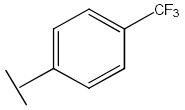	12.5	**BOT**	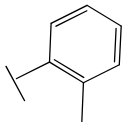	6.25
BPF	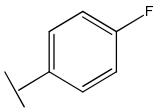	50	**BPN**	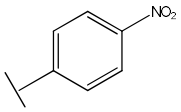	12.5
BOM	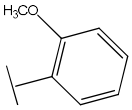	50	**BETX**	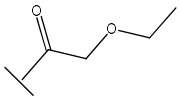	12.5
BMT	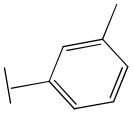	50	**BBN**	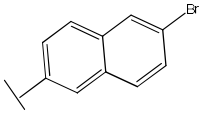	25
BPT	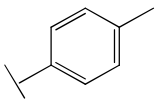	25	**BDP**	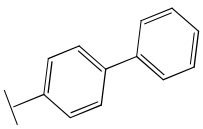	25
BDF	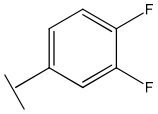	6.25	**BPM**	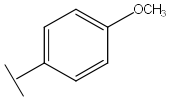	6.25

4.2 Anti-inflammatory activity:

The anti-inflammatory activity of synthesized (BOT, BDF and BPT) compounds was done and their percentage protection was calculated and presented inTable4. The findings showed that during the entire period of observation, the compounds tested at 10 mg/kg significantly reduced the edema. In comparison to BOT substance, the compounds BDF and BPT showed the highest percentage inhibition of edema. After 12hr compound BOT shown 84.43% inhibition of edema and compounds BDF and BPT produced 89.90 and 90.52% respectively.

Table 4. Anti-inflammatory activity of synthesized compounds using carrageenan induced rat paw edema in wistar rats.

Treatment group	Edema(mean ±SEM)								Edema inhibition (%)							
	30 min	1 h	2h	3 h	4h	6 h	12h	24 h	30 min	1 h	2h	3 h	4h	6 h	12h	24 h
DC	9.96 ± 0.01	0.21 ± 0.08	0.46± 0.19	0.52± 0.21	0.49± 0.20	3.38± 0.15	0.35± 0.14	0.06± 0.02	-	-	-	-	-	-	-	-
Std	6.18 ± 0.05	3.58 ± 0.15	1.96± 0.07	1.24± 0.03	0.57± 0.03	0.49± 0.008	0.17± 0.01	3.82± 0.02	37.86	48.49	67.86	77.03	87.13	89.09	97.15	81.36
BOT	8.52 ± 0.07	4.80 ± 0.14	3.41± 0.08	2.44± 0.07	1.51± 0.08	1.05± 0.01	0.93± 0.05	4.31± 0.01	14.45	30.91	43.92	54.92	66.36	75.98	84.43	60.94
BDF	7.85 ± 0.03	4.56 ± 0.11	3.11± 0.12	2.20± 0.02	1.46± 0.05	0.93± 0.05	0.61± 0.09	3.95± 0.006	21.16	34.40	49.08	59.12	67.44	79.42	89.80	75.43
BPT	7.80 ± 0.02	4.80 ± 0.14	2.71± 0.13	1.48± 0.04	0.89± 0.03	0.60± 0.02	0.56± 0.05	4.12± 0.012	20.73	30.91	55.60	72.67	80.09	86.45	90.52	68.16

Data represent mean ± SEM (n=6)
One-way ANOVA was used to analyse the data, and then Tukey's test was carried out.
ns = non significant when compared to disease control (DC)

4.3 Analgesic activity (Hot plate method):

When compared to the normal control, BOT, BDF, and BPT showed the highest levels of activity among all evaluated compounds. In general, Table 5 shows that the ortho-toluene containing compounds showed excellent analgesic activity while the other compounds displayed intermediate activity. All of the investigated compounds showed activity against analgesia, and these findings suggest that this core moiety might provide effective scaffolds for analgesic drugs. However, further testing is required to employ them for clinical usage despite the fact that this is a very promising preliminary study.

Table 5. Analgesic activity of selected synthesized heterocyclic compounds against Eddy's hot plate method.

Time min	STD	BOT	BDF	BPT
15	3.51±0.25^{ns}	3.43±0.06^{ns}	3.45±0.07^{ns}	3.45±1.92^{ns}
30	5.63±0.13****	3.56±0.07****	3.43±0.04****	3.51±1.28****
60	5.58±0.16****	3.86±0.07****	3.55±0.03****	3.61±3.17****
90	6.27±0.12 ****	4.03±0.05^{ns}	3.91±0.06^{ns}	4.00±2.83^{ns}
120	6.19±0.22 ****	4.68±0.10^{ns}	4.22±0.13^{ns}	4.15±3.03^{ns}
150	5.51±0.14****	3.61±0.10 *	4.02±0.08^{ns}	3.48±1.41**
180	4.47±0.16****	3.32±0.03*	3.73±0.09^{ns}	3.63±2.70^{ns}
210	3.02±0.10^{ns}	3.32±0.06^{ns}	3.42±0.05^{ns}	3.43±1.78^{ns}

All the values were represented as mean ±SEM, n=6
One-way ANOVA was used to analyse the data, and then Tukey's test was carried out.
p-value: *p<0.05, **p<0.01, ***p<0.001, ****p<0.0001, ns p>0.05 followed by Tukey's test

4.4 Investigation of Physicochemical and ADMET Properties:

Based on the anticipated outcomes summarized in Table 6 and 7, drug-likeness properties showed that compound BPF, BOM, BMT, BPT, BOT, BPN, BETX and BPM obeyed to Lipinski's rule with 0 violation and compound BCF, BDF, BBN and BDP passes with one violation MLOGP >4.15. The topological polar surface area was correlated to passive molecule transport across membranes as well as the BBB. The compounds having tPSA value < 140 Å2 passes the GI absorption standard. The entire tested molecules have tPSA value < 140Å2 hence passes the GI absorption standard and according to the yolk of Boiled-egg all other compounds except BPN are passively permeate through the blood-brain barrier (tPSA > 90.00 Å2). All of the derivatives' synthetic accessibility scores fell into the easy range (< 5). All of the tested molecules demonstrated HIA values and met the 30% requirement. The entire derivatives were non-Pgp substrates. These compounds were found to be inhibitors of CYP1A2 and CYP2C19 and also inhibitors of CYP2C9 except BETX. The derivatives of indazole were found to be no inhibitors of CYP2D6.

Table 6. ADMET Properties:

Compd. code	GI abs.	BBB permeant	Pgp substrate	BA value	CYP1 A2 inhibitor	CYP2 C19 inhibitor	CYP2 C9 inhibitor	CYP2 D6 inhibitor
BCF	High	Yes	No	0.55	Yes	Yes	Yes	No
BPF	High	Yes	No	0.55	Yes	Yes	Yes	No
BOM	High	Yes	No	0.55	Yes	Yes	Yes	No
BMT	High	Yes	No	0.55	Yes	Yes	Yes	No
BPT	High	Yes	No	0.55	Yes	Yes	Yes	No
BDF	High	Yes	No	0.55	Yes	Yes	Yes	No
BOT	High	Yes	No	0.55	Yes	Yes	Yes	No
BPN	High	No	No	0.55	Yes	Yes	Yes	No
BETX	High	Yes	No	0.55	Yes	Yes	No	No
BBN	High	Yes	No	0.55	Yes	Yes	Yes	No
BDP	High	Yes	No	0.55	Yes	Yes	Yes	No
BPM	High	Yes	No	0.55	Yes	Yes	Yes	No

GI abs.: Gastrointestinal absorption; BBB: Blood Brain Barrier; BA: Biological availability

Table 7. Drug likeness Properties:

Compd Code	MW	TPSA	MLOGP	HBD	HBA	RO5	RB	SA
BCF	369.14	34.89	4.59	0	5	1	3	2.16
BPF	319.13	34.89	4.11	0	3	0	2	2.04
BOM	331.16	44.12	3.38	0	3	0	3	2.23
BMT	315.16	34.89	3.96	0	2	0	2	2.12
BPT	315.16	34.89	3.96	0	2	0	2	2.11
BDF	337.12	34.89	4.5	0	4	1	2	2.13
BOT	315.16	34.89	3.96	0	2	0	2	2.14
BPN	346.14	80.71	2.7	0	4	0	3	2.18
BETX	283.12	44.12	2.05	0	3	0	4	2.26
BBN	430.09	34.89	5.09	0	2	1	2	2.2
BDP	377.23	34.89	4.9	0	2	1	3	2.41
BPM	331.16	44.12	3.38	0	3	0	3	2.14

MW=Molecular Weight; tPSA= Total Polar Surface Area; HBD= Hydrogen Bond Donars; HBA= Hydrogen Bond Acceptors; RB=Rotatable bonds; SA= Synthetic Asseccibility; RO5: Rule of Five.

5. Conclusion

In this study, we performed synthesis and molecular docking of 1H-indazole derivatives to find out potential 2AQK inhibitors. All these indazole derivatives possessed good pharmacokinetic and drug likeness properties. In addition, were found to be potentially binds to 2AQK enzyme. A 100 ns MD simulation study was carried out to confirm the stability of potential inhibitors. The results of the MD simulation showed that the test compound BOT was significantly stable in the Enoyl-ACP reductase-2AQK active site. The compound BOT-2AQK post-dynamic MM-GBSA analysis revealed substantial binding affinities with each of its chosen targets. The compound BDF, BOT and BPM shows excellent activity against mycobacterium tuberculosis and compound BPT containing p-toluene group shows highest anti-inflammatory and analgesic activity. Still more research is required to figure out whether indazole derivatives are effective in human clinical trials.

Acknowledgements: Authors are thankful to the Management of Dr. Vishwanath Karad MIT-World Peace University, Pune, India for the support. (Formerly MAEER's Maharashtra Institute of Pharmacy, Pune-411038). Authors are grateful to DST-SERB for financial support of this research.

Conflict of Interest:

The authors declare no conflicts of interest.

6. References

1. https://www.who.int/teams/global-tuberculosis-programme/tb reports/globaltuberculosis-report-2022 Assessed on 24 Jan. 2023.
2. Navisha Dookie, Santhuri Rambaran, Nesri Padayatchi, Sharana Mahomed and Kogieleum Naidoo. Evolution of drug resistance in Mycobacterium tuberculosis: a review on the molecular determinants of resistance and implications for personalized care. *J Antimicrob Chemother,* 2018; 73: 1138–1151.
3. Kantlam Chamakuri, Srinivasa Murthy Muppavarapu, Narsimha Reddy Yellu, Synthesis and analgesic and anti-inflammatory activities of 7-azaindazolechalcone derivatives. *Med Chem Res,* 2016; 1671-2.
4. Salvatore P, Demetrio R, Fabiana P, Casula G, Maggio B, Daidone G, Raimondi MV, Cusimano MG, Bombieri G, Meneghetti F. Synthesis and biological evaluation of new indazole derivatives. ARKIVOC, 2010(x):163–177.
5. Upadhyay A, Srivastava S, Yadav R. Conventional as well as microwave assisted synthesis and antimicrobial screening of 4-aryl-3-chloro-1-[(5-nitroindazol-1-yl)acetamido]-2-oxo azetidines. *Ind J Chem*; 50:89–97.
6. Maggio B, Raimondi MV, Raffa D, Plescia F, Cascioferro S, Plescia S, Tolomeo M, Di Cristina A, Pipitone RM, Grimaudo S, Daidone G. Synthesis of substituted 3-amino-N-phenyl-1H-indazole- 1-carboxamides endowed with antiproliferative activity. *Eur J Med Chem*; 2011; 46:168–174.
7. Rudavath D, Sreenivasulu R, Raju R.R. Synthesis and antitumor evaluation of indole-substituted indole-fused keto hydrazide–hydrazones. J Pharm Res, 2018; 12:42–46.
8. Upul K. Bandarage, Michael P. Clark, Emanuele Perola, Huai Gao, Marc D. Jacobs, Alice Tsai, et al. Novel 2-Substituted 7-Azaindole and 7-Azaindazole Analogues as Potential Antiviral Agents for the Treatment of Influenza. *ACS Med. Chem. Lett.* 2017; *8*(2):261-265.
9. Violina T. Angelova, Tania Pencheva, Nikolay Vassilev, Rumyana Simeonova, Georgi Momekov, Violeta Valcheva. New indole and indazole derivatives as potential antimycobacterial agents. *Med Chem Res.,* 2019; 28(4): 485–497.
10. Park Y, Pacitto A, Bayliss T, Cleghorn LA, Wang Z, Hartman T, Arora K,

Ioerger TR, Sacchettini J, Rizzi M. Essential but not vulnerable: indazole sulfonamides targeting inosine monophosphate dehydrogenase as potential leads against Mycobacterium tuberculosis. *ACS Infect Dis.*, 2016; 3:18–33.

11. Malapati P, Krishna VS, Dharmarajan S. Identification and development of novel indazole derivatives as potent bacterial peptidoglycan synthesis inhibitors. *Int J Mycobact.*, 2018; 7(1):76-83.
12. Lee F, Cherng J, Huang L, Huang T, Tsai S-C, Teng C-M, Wu C-C, Cheng F-C, Kuo S-C Synthesis of 1-benzyl-3-(5′-hydroxymethyl- 2′-furyl)indazole analogues as novel antiplatelet agents. *J Med Chem.,* 2001; 44(22):3746–3749.
13. Kevin G, Albert J, Robichaud A, Alexander A, Greenfield A, Lo JR, Grosanu C, Mattes JF, Cai Y, Zhang GM, Zhang JY, Kowal DM, Smith DL, Di L, Kerns EH, Schechter LE, Comery TA. Identification of 3-sulfonylindazole derivatives as potent and selective 5-HT6 antagonists. *Bioorg Med Chem*., 2011; 19(1):650–662.
14. N O'Boyle. M Bank, C A James, C Morley, T Vandermeersch and G R Hutchison. Open Bable: An open chemical toolbox. *J. Cheminform.,* 2011; 3:33.
15. Pettersen EF, Goddard TD, Huang CC, Couch GS, Greenblatt DM, Meng EC, Ferrin TE. UCSF Chimera-visualization system for exploratory research and analysis. *J.Comput.Chem.*, 2004;25(13): 1605-12.
16. Forli, S., Huey, R., Pique, M. E., Sanner, M. F., Goodsell, D. S., & Olson, A. J. Computational protein–ligand docking and virtual drug screening with the AutoDock suite. *Nat. Protoc*., 2016; 11(5): 905–919.
17. Ferreira, L., dos Santos, R., Oliva, G., & Andricopulo, A. Molecular Docking and Structure-Based Drug Design Strategies.*Molecules*,2015;20(7):13384 –13421.
18. J.S. Oliveira, J.H. Pereira, F. Canduri, N.C. Rodrigues, O.N. de Souza, W.F. de Azevedo, L.A. Basso and D.S. Santos. Crystallographic and Pre-steady-state Kinetics Studies on Binding of NADH to Wild-type and Isoniazid-resistant Enoyl-ACP(CoA) Reductase Enzymes from *Mycobacterium tuberculosis***.** *J. Mol. Biol*., 2006; 359(3):646-66.
19. Duggan, K.C., Walters, M.J., Musee, J., Harp, J.M., Kiefer, J.R., Oates, J.A., Marnett, L.J. Molecular basis for

cyclooxygenase inhibition by the non-steroidal anti-inflammatory drug naproxen. *J. Biol. Chem*., 2010; 285(45): 34950-34959.

20. Shaw DE, Maragakis P, Lindorff-Larsen K, Piana S, Dror RO, Eastwood MP, Bank JA, Jumper JM, Salmon JK, Shan Y, Wriggers W. Atomic-level characterization of the structural dynamics of proteins. *Science,* 2010; 330(6002):341-6.
21. Bowers KJ, Chow DE, Xu H, Dror RO, Eastwood MP, Gregersen BA, Klepeis JL, Kolossvary I, Moraes MA, Sacerdoti FD, Salmon JK. Scalable algorithms for molecular dynamics simulations on commodity clusters. InSC'06: Proceedings of the 2006 ACM/IEEE Conference on Supercomputing, 2006; 43-43.
22. Chow E, Rendleman CA, Bowers KJ, Dror RO, Hughes DH, Gullingsrud J, Sacerdoti FD, Shaw DE. Desmond performance on a cluster of multicore processors. DE Shaw Research Technical Report DESRES/TR-2008-01.
23. Shivakumar, D., Williams, J., Wu, Y., Damm, W., Shelley, J., & Sherman, W. Prediction of Absolute Solvation Free Energies using Molecular Dynamics Free Energy Perturbation and the OPLS Force Field. *J. Chem. Theory Comput*., 2010; 6(5): 1509–1519.
24. Jorgensen, W. L., Chandrasekhar, J., Madura, J. D., Impey, R. W., & Klein, M. L. Comparison of simple potential functions for simulating liquid water. *J. Chem. Phys*., 1983; 79(2): 926–935.
25. Martyna, G. J., Tobias, D. J. & Klein, M. L. Constant pressure molecular dynamics algorithms. *J. Chem. Phys.*, 1994; 101(5): 4177–4189.
26. Martyna, G. J., M. L. Klein, and M. Tuckerman. Nose-Hoover chains-the canonical ensemble via continuous dynamics. *J. Chem. Phys.*, 1992; 97(4): 2635–2643.
27. Abdulnour Y. Toukmaji, John A. Board, Ewald summation techniques in perspective: a survey, Computer Physics Communications, 1996; 95(2–3):73-92,
28. Lipinski C. A., Lombardo F., Dominy B. W. & Feeney P.J. Experimental and computational approaches to estimate solubility and permeability in drug discovery and development settings. *Adv. Drug Deliv. Rev*., 2001; 46(1-3):3–26.
29. Daina A., Michielin O. & Zoete V. SwissADME: a free web tool to evaluate pharmacokinetics, druglikeness and medicinal chemistry friendliness of

small molecules. *Sci. Rep.,* 2017; 7(1):42717.

30. Ertl, P., Schuffenhauer A. Estimation of synthetic accessibility score of drug-like molecules based on molecular complexity and fragment contributions. *J. Cheminform*., 2009; 1:8.
31. Ertl, P., Rohde, B. & Selzer, P. Fast. Calculation of molecular polar surface area as a sum of fragment-based contributions and its application to the prediction of drug transport properties. *J. Med. Chem.,* 2000; 43:3714–3717.
32. Daina, A. & Zoete, V. A BOILED-Egg to Predict Gastrointestinal Absorption and Brain Penetration of Small Molecules. *Chem Med Chem*., 2016; 11:1117–1121.
33. P. D. Lokhande, Abdul Raheem, S. T. Sabale, A. R. Chabukswar and S. C. Jagdale. An efficient synthesis of 1-H indazoles. *Tetrahedron Lett.;* 2007; 48(49): 6890–6892.
34. Xing-Rong Wang, Shuai Wang, Wen-Bo Li, Kai-Yan Xu, Xue-Peng Qiao, Xue-Li Jing, et al. Design, synthesis and biological evaluation of novel 2-(4-(1H-indazol-6-yl)-1H-pyrazol-1yl)acetamide derivatives as potent VEGFR-2 inhibitors. *Eur J Med Chem.*, 2021; 213:113192.